Shell Filling and Paramagnetism in Few Electron Colloidal Nanoplatelets

Jordi Llusar[1] and Juan I. Climente[1]

[1]*Departament de Química Física i Analítica, Universitat Jaume I, E-12080, Castelló de la Plana, Spain*

(Dated: June 30, 2022)

Colloidal semiconductor nanoplatelets are excellent optical emitters, which combine a quasi-2D structure with strong in-plane Coulomb interactions. Here we go beyond the photoexcitation regime and investigate theoretically the effect of charging nanoplatelets with a few interacting fermions (electrons or holes). This introduces severe Coulomb repulsions in the system, enhanced by the inherent dielectric confinement. We predict strong electronic correlations and electron-electron exchange energies (over 20 meV) in type-I (CdSe/CdS) and type-II (CdSe/CdTe) nanoplatetets, which give rise to characteristic physical phenomena. These include shell filling spectra deviating from the Aufbau principle, large addition energies which permit deterministic control of the number of charges at room temperature and paramagnetic electron spin configuration activated at cryogenic temperatures.

The number of excess carriers (electrons or holes) confined in semiconductor quantum dots is analogous to the charge number of ions in chemistry. Because changes in this number are expected to modify the electronic properties, experiments in the early years of quantum dots struggled to control it. Orbital shell filling was subsequently demonstrated in gated[1], self-assembled[2–4], carbon nanotube[5] and graphene[6] quantum dots. In colloidal nanocrystal quantum dots, orbital shell filling of conduction and valence bands was pursued using different approaches such as scanning tunneling spectroscopy[7], direct or remote doping[8] and electrochemical injection.[9] The placement of resident charges in the nanocrystals translated into substantial changes of the transport and optical properties, including lower threshold optical gain[10] and large electrochromic shifts,[11, 12] which are of interest for lasing and sensing applications, respectively.

Recently, progress in electrochemical charge injection has reached deterministic and stable control of the number of confined carriers in individual nanocrystals.[13] Charge control through doping (with impurities or surrounding molecules) is advancing in this direction,[14–16] and scanning tunneling spectroscopy[7, 17, 18] in the shell-filling regime can be expected to do so as well. These achievements open path for a precise analysis of the shell structure, potentially unveiling few-body charge and spin interaction effects at a level so far restricted to fully solid state systems. In nanocrystal quantum dots, quantum confinement energies usually prevail over Coulomb interaction energies.[19] This is a similar situation to that of epitaxial quantum dots. One can then expect orbital shell filling to be simply understood from the dot geometry, following Hund and Aufbau rules, with many-body interactions acting as a perturbation.[1, 2, 20, 21] A different scenario can however be foreseen for nanoplatelets (NPLs). These are often considered the colloidal analogous of epitaxial quantum wells, albeit with finite and controllable lateral confinement, the possibility to develope in-plane (core/crown) heterostructures and a strong dielectric confinement imposed by the organic ligands.[22]

The flexible design and outstanding optical properties of colloidal NPLs have triggered intensive research over the last years aiming at applications in optoelectronic devices.[15, 23–26] Much of the interest follows from the strong attraction between photogenerated electron-hole pairs, enhanced by the quasi-2D geometry and the dielectric confinement, which prompt large binding energies (150-250 meV) and fast radiative recombination rates through the so-called giant oscillator strength effect.[22, 27–30] One should however note that the same factors that favor strong electron-hole attraction, favor strong electron-electron or hole-hole repulsion too. In NPLs with injected carriers, these interactions ($\sim$ 100 meV) largely exceed the small energy spacings between states of non-interacting particles, which are set by the weak lateral confinement ($\sim$ 10 meV). The resulting shell structure can then be expected to display non-trivial many-body phenomena.[3, 4, 31] Possible implications of an electronic structure shaped by strong repulsive correlations include the buildup of intrinsic ferromagnetism and exotic spin states.[31–33]

In order to investigate these effects, we study CdSe-based NPLs of current interest. Specifically, we model CdSe/CdS and CdSe/CdTe core/crown heterostructures,[22] see schematics in Figures 1a and 1d, respectively. Similar behavior can be expected for core-only and core/shell NPLs, but the crown passivates lateral facets, which are prone to formation of traps,[34] and the use of shells gradually quenches dielectric confinement, which is needed to reach the strong correlation regime we report.

To visualize the role of Coulomb repulsions we will conjugate two competing degrees of freedom: the number of confined carriers and the quantum confinement strength. Thus, we take a fixed crown (lateral dimensions 20×30 nm^2), and change the core size (lateral dimensions $10 \times L_y^c$ nm^2, where $L_y^c = 12 - 20$ nm is the length of the core). The NPL thickness is 4.5 monolayers. These are typical

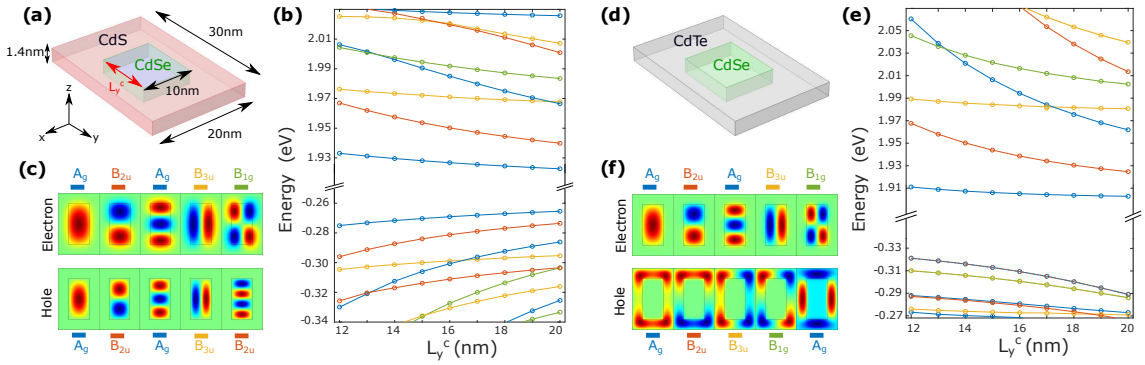

FIG. 1: (a) Schematic of the CdSe/CdS NPLs under study. (b) Non-interacting electron (top) and hole (bottom) energy levels as a function of the core length. (c) Wave functions of the lowest electron (highest hole) energy levels for $L_y^c = 20$ nm. (d-f): same but for CdSe/CdTe NPLs. The NPLs have the same dimensions as for CdSe/CdS. All energies are referred to the top of the CdSe valence band. The colors of the lines in (b), (c), (e) and (f) denote the irreducible representation of the level (within the D_{2h} point group).

values for this kind of structure.[35]

It is convenient to start by analyzing the energy structure of non-interacting electrons and holes, which we calculate using effective mass Hamiltonians including strain and dielectric mismatch terms (see Supporting Information, SI). In CdSe/CdS NPLs, the first electron and hole states localize in the core (Fig. 1c), but in CdSe/CdTe NPLs the hole moves towards the crown (Fig. 1f), as expected from the type-I vs type-II band alignment. The energy dependence on the core length is similar for all particles localized within it. For instance, Fig. 1b shows that increasing L_y^c in CdSe/CdS NPLs has little influence on the electron or hole ground state energy (A_g symmetry) because the lateral confinement is already weak. However, some of the excited states (those with nodes along the y axis) are more sensitive to the confinement relaxation and lower their energy more, see e.g. the first excited state (B_{2u} symmetry). The same happens for electrons in CdSe/CdTe NPLs, as can be seen in Fig. 1e (top part). This is an indication that the NPL core is not yet in the quantum well limit,[18] and hence the density of states can be increased by making it larger. The smaller interlevel energy spacings will translate into stronger electronic correlation effects, as we shall show below.

For holes in CdSe/CdTe, the behavior is different because increasing the core size reduces the space left in the crown. This unstabilizes the energy levels for large L_y^c values. It is also worth noting that the top-most levels of the valence band are formed by nearly degenerate pairs of states (A_g and B_{2u}, B_{3u} and B_{1g}). This is because the core constitutes a potential barrier which separates the crown into two symmetric sides. The pairs of levels are the symmetric and antisymmetric solutions of the double box system. The top-most hole states have little kinetic energy, so that tunneling is weak and the two solutions are quasi degenerate.[36] This is a diatomic-like system, where characteristic interactions –different from those of quantum dots– can be expected.

We are now in a position to study the orbital shell filling of the NPLs. To this end, we calculate the addition energy (the analogous of electron affinity in real atoms) spectrum for the two first conduction and valence band shells (i.e. up to 4 electrons or 4 holes). The addition energy is the energy required to insert one additional charge into the nanostructure:[1]

$$\Delta = \mu(N+1) - \mu(N) = E(N+1) - 2E(N) + E(N-1). \quad (1)$$

where $\mu(N)$ and $E(N)$ are the chemical potential and ground state energy for N carriers (electrons or holes). $E(N)$ values are extracted from full configuration interaction (CI) calculations on the basis of the single-particle spin-orbitals (see SI).

Fig. 2a shows the addition energies one would expect for non-interacting electrons in a core with $L_y^c = 20$ nm. In this case, a simple orbital shell filling sequence is observed. Odd numbers of electrons (N_e) involve half-filled (open) shell. Because we are neglecting Coulomb interactions so far, introducing an extra electron in these cases requires no additional energy, $\Delta = 0$ meV. By contrast, even numbers of electrons involve closed shells. Introducing an extra electron requires providing the energy to access the next excited orbital, which is set by the lateral quantum confinement or in other words, it is due to the inter-level spacing separation observed in Fig. 1b,e. This results in $\Delta \approx 20$ meV.

Upon inclusion of Coulomb interactions, major changes take place in the electron addition spectrum. Fig. 2b show the spectrum in the absence of dielectric confinement (assuming the outer medium has the same dielectric constant as the NPL, $\varepsilon_{out} = \varepsilon_{in}$). This situation can be expected in NPLs with thick shells and is reminiscent of epitaxial quantum dots. Open shells have now addition energies $\Delta = 25 - 30$ meV, which give

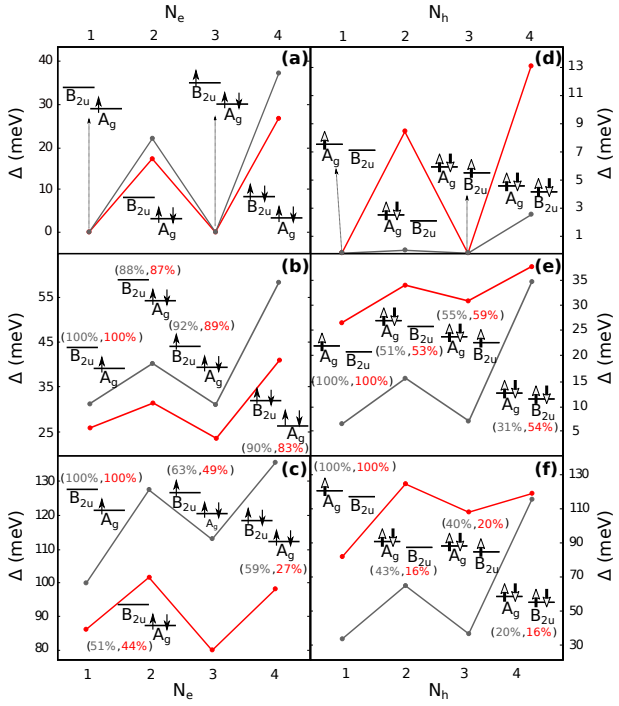

FIG. 2: Addition energy spectra as a function of the number of carriers for CdSe/CdS (red line) and CdSe/CdTe (gray line) in a NPL with $L_y^c = 20$ nm. (a) Non-interacting electrons. (b) Interacting electrons neglecting dielectric confinement ($\varepsilon_{out} = \varepsilon_{in}$). (c) Interacting electrons including dielectric confinement ($\varepsilon_{out} = 2$). (d-f) Same for holes. The insets show the dominant electronic configuration along with its weight in the CI expansion (red value for CdSe/CdS, gray one for CdSe/CdTe).

a direct measure of the electron-electron repulsions one needs to overcome in order to place an extra electron in the same orbital. Closed shells are still more stable than open ones, but Coulomb repulsions are less severe when the extra electron is placed in a different (orthogonal) orbital. Consequently, the sawtooth structure in Fig. 2b is less pronounced than one would expect from quantum confinement alone (Fig. 2a). When dielectric confinement is added ($\varepsilon_{out} < \varepsilon_{in}$), which provides a realistic description of NPLs with no shell, Coulomb repulsions are greatly enhanced (roughly tripled), yielding Δ values over 80 meV, see Fig. 2c. It is worth noting that the Δ shift between non-interacting and interacting cases is not constant against the number of carriers (see Fig. S1 in the SI). This is a first indication that we are beyond the perturbative Coulomb regime, and electronic correlations play a significant role. The latter effect is particularly remarkable in CdSe/CdS NPLs with cores under $L_y^c = 15$ nm, where anomalous shell filling spectra can be observed, with closed shell configurations being less stable than open ones, see Fig. S2.

For holes, the impact of Coulomb interactions is also drastic. Holes in CdSe/CdS NPLs behave much like electrons in spite of the heavier masses, see red line in Fig. 2d-f. Holes in CdSe/CdTe behave differently instead because they are localized in the crown, see gray lines in the figure. In a non-interacting picture, Fig. 2d, $\Delta \approx 0$ meV for a number of holes $N_h = 1 - 3$, but $\Delta = 2.8$ meV for $N_h = 4$. This reflects the valence band electronic structure analyzed in Fig. 1f. The top-most hole orbitals (A_g and B_{2u}) are quasi degenerate. Together with the spin degree of freedom, this gives a four-fold quasi-degenerate ground state. Then, adding extra holes requires very little energy except for the closed shell, $N_h = 4$. However, when repulsions are taken into account (Figs. 2e,f), all addition energies shift up and a peak emerges for $N_h = 2$. The latter is because two holes feel comfortable sitting on opposite sides of the crown, but adding a third hole necessarily implies stronger repulsions.

The insets in Fig. 2 show, for each N_e or N_h value, the electronic configuration which is expected to dominate from the Aufbau principle of atoms, i.e. assuming that independent-particle spin-orbitals are filled sequentially. For interacting particles, the percentage gives the weight of such a configuration within the CI expansion. In the absence of dielectric mismatch, Figs. 2b,e, this is indeed the dominant configuration (weights over 50%). This is especially true for electrons, while holes are in a regime of stronger correlations, consistent with earlier studies on epitaxial quantum dots.[3, 4, 31] Upon inclusion of dielectric mismatch, however, correlations become even stronger, which is manifested as weights below 50% in Figs. 2c,f. That is, the configuration expected from the Aufbau principle is no longer the dominant one, and it misses most of the electronic structure details.

It is concluded from Fig. 2 that Coulomb repulsions play a dominant role in shaping the electronic structure and addition energy spectrum of electrons and holes in NPLs. This is so in spite of the large in-plane dimensions, which in principle allow fermions to localize far from each other to minimize interactions (as in incipient Wigner crystals[37]). An important practical consequence is that, owing to dielectric confinement, all Δ values exceed thermal energy at room temperature. This implies that electrochemical charging of NPLs[38] is susceptible of being conducted electron-by-electron (or hole-by-hole), thus enabling deterministic control of the number of charges in spite of the weak lateral confinement. The same conclusion holds for different core dimensions (Fig.S2).

The results so far also reveal that electrons in CdSe cores can experience severe correlations, because Coulomb repulsions are up to one order of magnitude larger than the interlevel energy spacing set by lateral confinement ($\sim$ 100 meV against $\sim$ 10 meV for $L_y^c = 20$ nm). These are potentially suitable conditions for the formation of magnetic phases.[39, 40] Confirming such a point is of significant interest, since ear-

lier manifestations of magnetic phases in colloidal NPLs were restricted to doping[24, 41–44] and surface-induced paramagnetism.[45] The development of intrinsic magnetism would open up new scenarios for spintronic and magnetic devices.

To explore this possibility, in Fig. 3 we plot the energy difference between low and high spin states of few-electron ($N_e = 2-4$) CdSe/CdS NPLs and the associated expectation values of the total spin quantum number (similar results hold for CdSe/CdTe, Fig. S3). Fig. 3a shows the energy splitting between the $N_e = 2$ ground state (singlet, $S_e = 0$) and the first excited state (triplet, $S_e = 1$). Clearly, as the core size increases, the triplet approaches the singlet ground state. There are two reasons for this. One is the weakening of lateral confinement, which selectively relaxes the first excited orbital (B_{2u}, p_y-like) but not the lowest one (A_g, s-like), as discussed before in Fig. 1. The other reason is that strong Coulomb repulsions imply large Coulomb exchange energies as well, which stabilize triplets as compared to singlets. Fig. 3a compares the triplet energy for two non-interacting (dotted line) and two interacting (solid line with black circles) electrons. The energy decrease for non-interacting electrons is merely due to the weakened confinement, while that of the interacting case further benefits from exchange energies as large as $20-30$ meV. Consequently, for two interacting electrons, the $S_e = 1$ state is only 8 meV away from the $S_e = 0$ ground state when $L_y^c = 12$ nm, and is nearly degenerate when $L_y^c = 20$ nm. It follows that thermal occupation of high spin states is feasible at room temperature or even earlier. This is evidenced by Fig. 3b. With increasing temperature, the total spin $\langle S_e \rangle$ rapidly departs from $\langle S_e \rangle = 0$ (pure singlet), which is the value one would obtain in strongly confined nanocrystals, and reaches $\langle S_e \rangle \approx 3/4$, which implies equal population of singlet and triplet states. For large cores ($L_y^c = 20$ nm), this is achieved at temperatures under 50 K. The practical implication is that paramagnetic response must be expected except at temperatures $T \to 0$ K.

The ground state of a $N_e = 2$ system in the absence of external magnetic fields or spin-orbit interaction is always spin-singlet.[40] In Fig. 3c,d we explore whether this situation can be reversed for $N_e = 3-4$ NPLs, and high-spin ground states show up. For the geometries we address the answer is negative (at $T = 0$ K the spin is low). but again high-spin states are occupied at room temperature. In fact, for $N_e = 4$ and 300K we obtain $\langle S_e \rangle > 3/4$, see Fig. 3d. That is, thermal population of triplet states exceeds that of singlet ones. The reason is that more than one triplet state becomes reachable at room temperature, see Fig. S3.

Solid and dashed lines in Fig. 3 refer to estimates including and excluding dielectric confinement. It is clear from the comparison that the spin momenta are higher when the inhomogeneous dielectric screening is taken into account, which is a reflection of the greater Coulomb exchange energies.

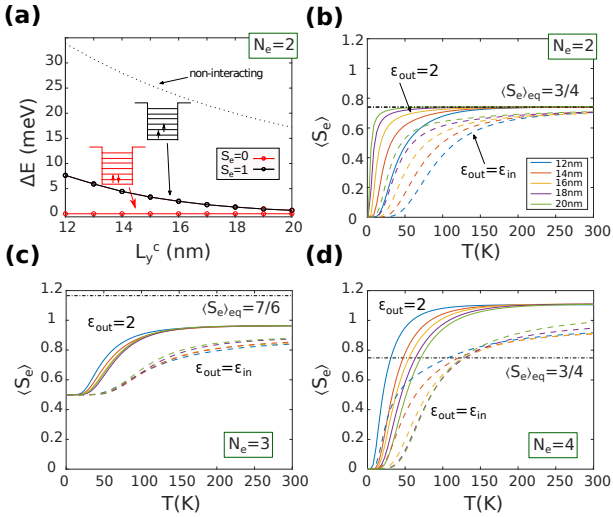

FIG. 3: (a) Energy splitting between ground state (singlet) and the first excited state (triplet) for two electrons in CdSe/CdS NPL with varying core length. The insets illustrate the main electronic configuration for each state. The dotted line in (a) represents the triplet state of two non-interacting electrons, for comparison. (b-d): expectation value of total electron spin as a function of the temperature for different core lengths, with two (b), three (c) and four (d) electrons. $\langle S_e \rangle_{eq}$ is the value for equal number of low and high spin states populated. Solid (dashed) lines are used for calculations including (excluding) dielectric confinement.

We conclude from Fig. 3 that the large Coulomb exchange energy and the weak lateral confinement of colloidal NPLs enable the occupation of high spin states from cryogenic temperatures, which should provide few-electron NPLs with paramagnetic behavior in most practical instances. Because the total spin of electrons couples to that of magnetic dopants and to external fields,[24, 45] these findings anticipate that charged NPLs will display enhanced magnetic response, modulable through the number of injected carriers.[46, 47] They can also be used to explore spin oscillation phenomena[48] and optical orientation protocols differing from those of NPLs with conventional photoexcitation of neutral excitons.[45, 49]

In summary, we have shown that the number of fermions (electrons or holes) confined in colloidal NPLs sparks profound changes on the electronic structure. The strong Coulomb repulsions and the weak lateral confinement of NPLs combine to yield a regime of strong electronic correlations, producing non-trivial physical effects. These include (i) violations of the Aufbau principle; (ii) addition energies over 30 meV, which imply the feasibility of charging NPLs carrier-by-carrier at room temperature despite the weak lateral confinement; (iii) thermal occupation of high-spin states, enabled by the strong

Coulomb exchange energies ($20-35$ meV), which implies that magnetic interactions with external fields or dopants will be greatly enhanced in multi-electron and multi-hole systems.

The authors acknowledge support from MICINN PID2021-128659NB-I00 and UJI-B2021-06 projects. We are grateful to Josep Planelles, Iwan Moreels, Thierry Barisien, Louis Biadala and Nemanja Peric for discussions.

[1] S. Tarucha, D. Austing, T. Honda, R. Van der Hage, and L. P. Kouwenhoven, Physical Review Letters **77**, 3613 (1996).
[2] H. Drexler, D. Leonard, W. Hansen, J. Kotthaus, and P. Petroff, Physical Review Letters **73**, 2252 (1994).
[3] D. Reuter, P. Kailuweit, A. Wieck, U. Zeitler, O. Wibbelhoff, C. Meier, A. Lorke, and J. Maan, Physical review letters **94**, 026808 (2005).
[4] M. Ediger, G. Bester, A. Badolato, P. Petroff, K. Karrai, A. Zunger, and R. Warburton, Nature Physics **3**, 774 (2007).
[5] H. I. Jørgensen, K. Grove-Rasmussen, K.-Y. Wang, A. Blackburn, K. Flensberg, P. Lindelof, and D. Williams, Nature Physics **4**, 536 (2008).
[6] J. Güttinger, T. Frey, C. Stampfer, T. Ihn, and K. Ensslin, Physical review letters **105**, 116801 (2010).
[7] E. Bakkers, Z. Hens, A. Zunger, A. Franceschetti, L. Kouwenhoven, L. Gurevich, and D. Vanmaekelbergh, Nano Letters **1**, 551 (2001).
[8] D. J. Norris, A. L. Efros, and S. C. Erwin, Science **319**, 1776 (2008).
[9] P. Guyot-Sionnest, Microchimica Acta **160**, 309 (2008).
[10] K. Wu, Y.-S. Park, J. Lim, and V. I. Klimov, Nature Nanotechnology **12**, 1140 (2017).
[11] C. Wang, M. Shim, and P. Guyot-Sionnest, Science **291**, 2390 (2001).
[12] S. Brovelli, W. K. Bae, C. Galland, U. Giovanella, F. Meinardi, and V. I. Klimov, Nano letters **14**, 486 (2014).
[13] S. Morozov, E. L. Pensa, A. H. Khan, A. Polovitsyn, E. Cortés, S. A. Maier, S. Vezzoli, I. Moreels, and R. Sapienza, Science advances **6**, eabb1821 (2020).
[14] C. Capitani, V. Pinchetti, G. Gariano, B. Santiago-González, C. Santambrogio, M. Campione, M. Prato, R. Brescia, A. Camellini, F. Bellato, *et al.*, Nano letters **19**, 1307 (2019).
[15] A. Dutta, A. Medda, and A. Patra, The Journal of Physical Chemistry C (2020).
[16] B. T. Diroll, W. Cho, I. Coropceanu, S. M. Harvey, A. Brumberg, N. Holtgrewe, S. A. Crooker, M. R. Wasielewski, V. B. Prakapenka, D. V. Talapin, *et al.*, Nano letters **18**, 6948 (2018).
[17] D. Katz, O. Millo, S.-H. Kan, and U. Banin, Applied Physics Letters **79**, 117 (2001).
[18] N. Peric, Y. Lambert, S. Singh, A. H. Khan, N. A. Franchina Vergel, D. Deresmes, M. Berthe, Z. Hens, I. Moreels, C. Delerue, *et al.*, Nano Letters **21**, 1702 (2021).
[19] A. Piryatinski, S. A. Ivanov, S. Tretiak, and V. I. Klimov, Nano letters **7**, 108 (2007).
[20] S. Nagaraja, P. Matagne, V.-Y. Thean, J.-P. Leburton, Y.-H. Kim, and R. M. Martin, Physical Review B **56**, 15752 (1997).
[21] R. Warburton, B. T. Miller, C. Dürr, C. Bödefeld, K. Karrai, J. Kotthaus, G. Medeiros-Ribeiro, P. Petroff, and S. Huant, Physical Review B **58**, 16221 (1998).
[22] M. Nasilowski, B. Mahler, E. Lhuillier, S. Ithurria, and B. Dubertret, Chemical reviews **116**, 10934 (2016).
[23] B. T. Diroll, Journal of Materials Chemistry C **8**, 10628 (2020).
[24] M. Sharma, S. Delikanli, and H. V. Demir, Proceedings of the IEEE **108**, 655 (2019).
[25] Y. Min, E. Im, G.-T. Hwang, J.-W. Kim, C.-W. Ahn, J.-J. Choi, B.-D. Hahn, J.-H. Choi, W.-H. Yoon, D.-S. Park, *et al.*, Nano Research **12**, 1750 (2019).
[26] B. Vasić, S. Aškrabić, M. M. Jakovljević, and M. Artemyev, Applied Surface Science **513**, 145822 (2020).
[27] A. W. Achtstein, A. Schliwa, A. Prudnikau, M. Hardzei, M. V. Artemyev, C. Thomsen, and U. Woggon, Nano Lett. **12**, 3151 (2012).
[28] F. Rajadell, J. I. Climente, and J. Planelles, Phys. Rev. B **96**, 035307 (2017).
[29] A. Naeem, F. Masia, S. Christodoulou, I. Moreels, P. Borri, and W. Langbein, Physical Review B **91**, 121302 (2015).
[30] S. J. Zelewski, K. C. Nawrot, A. Zak, M. Gladysiewicz, M. Nyk, and R. Kudrawiec, The journal of physical chemistry letters **10**, 3459 (2019).
[31] L. He, G. Bester, and A. Zunger, Physical review letters **95**, 246804 (2005).
[32] H. Tasaki, *Physics and mathematics of quantum many-body systems* (Springer, 2020).
[33] C. P. García, V. Pellegrini, A. Pinczuk, M. Rontani, G. Goldoni, E. Molinari, B. S. Dennis, L. N. Pfeiffer, and K. W. West, Physical review letters **95**, 266806 (2005).
[34] J. Leemans, S. Singh, C. Li, S. Ten Brinck, S. Bals, I. Infante, I. Moreels, and Z. Hens, The Journal of Physical Chemistry Letters **11**, 3339 (2020).
[35] S. Pedetti, S. Ithurria, H. Heuclin, G. Patriarche, and B. Dubertret, Journal of the American Chemical Society **136**, 16430 (2014).
[36] V. Steinmetz, J. I. Climente, R. Pandya, J. Planelles, F. Margaillan, Y. Puttisong, M. Dufour, S. Ithurria, A. Sharma, G. Lakhwani, L. Legrand, F. Bernardot, C. Testelin, M. Chamarro, A. Chin, A. Rao, and T. Barisien, The Journal of Physical Chemistry C **124**, 17352 (2020).
[37] V. Goldman, M. Santos, M. Shayegan, and J. Cunningham, Physical review letters **65**, 2189 (1990).
[38] B. T. Diroll, M. Chen, I. Coropceanu, K. R. Williams, D. V. Talapin, P. Guyot-Sionnest, and R. D. Schaller, Nature Communications **10**, 1 (2019).
[39] H. Tasaki, *Physics and mathematics of quantum many-body systems* (Springer, 2020).
[40] D. C. Mattis, *The theory of magnetism I: Statics and Dynamics*, Vol. 17 (Springer Science & Business Media, 2012).
[41] E. V. Shornikova, D. R. Yakovlev, D. O. Tolmachev, V. Y. Ivanov, I. V. Kalitukha, V. F. Sapega, D. Kudlacik, Y. G. Kusrayev, A. A. Golovatenko, S. Shendre, *et al.*, ACS nano **14**, 9032 (2020).
[42] A. H. Davis, E. Hofman, K. Chen, Z.-J. Li, A. Khammang, H. Zamani, J. M. Franck, M. M. Maye, R. W.

Meulenberg, and W. Zheng, Chemistry of Materials **31**, 2516 (2019).
[43] L. Dai, C. Strelow, T. Kipp, A. Mews, I. Benkenstein, D. Eifler, T. H. Vuong, J. Rabeah, J. McGettrick, R. Lesyuk, *et al.*, Chemistry of Materials (2020).
[44] A. Najafi, M. Sharma, S. Delikanli, A. Bhattacharya, J. R. Murphy, J. Pientka, A. Sharma, A. P. Quinn, O. Erdem, S. Kattel, *et al.*, The Journal of Physical Chemistry Letters **12**, 2892 (2021).
[45] E. V. Shornikova, A. A. Golovatenko, D. R. Yakovlev, A. V. Rodina, L. Biadala, G. Qiang, A. Kuntzmann, M. Nasilowski, B. Dubertret, A. Polovitsyn, *et al.*, Nature nanotechnology **15**, 277 (2020).
[46] J. Fernández-Rossier and L. Brey, Physical review letters **93**, 117201 (2004).
[47] F. Qu and P. Hawrylak, Physical Review Letters **95**, 217206 (2005).
[48] M. Wagner, U. Merkt, and A. Chaplik, Physical Review B **45**, 1951 (1992).
[49] J. Llusar and J. I. Climente, physica status solidi (b) , 2200081 (2022).

Supporting Information for "Shell Filling and Paramagnetism in Few Electron Colloidal Nanoplatelets"

Jordi Llusar and Juan I. Climente*

Departament de Química Física i Analítica, Universitat Jaume I, E-12080, Castelló de la Plana, Spain

E-mail: climente@uji.es

Theoretical model

Calculations are carried within the k·p theory framework. The Hamiltonian for N interacting particles (electrons or holes) reads:

$$\hat{H}_N = \sum_{i=1}^{N} \hat{h}_i + \frac{1}{2} \sum_{i,j \neq i}^{N} V_c(\mathbf{r}_i, \mathbf{r}_j), \tag{1}$$

where V_c terms account for repulsive Coulomb interactions, and $\hat{h}_i$ is a single-particle, single-band Hamiltonian for conduction electrons ($i = e$) or valence band heavy holes ($i = h$):

$$\hat{h}_i = \sum_{\alpha=x,y,z} \left(\frac{\hat{p}_\alpha^2}{2m_{i,\alpha}} + V_i(\mathbf{r}_i) \right). \tag{2}$$

In this equation, $\hat{p}_\alpha$ are the components of the 3-dimensional momentum operator, $m_{i,\alpha}$ those of the effective mass (anisotropic for holes), and V_i is a single-particle potential that can admit different kind of terms within it. In our calculations, the V_i term was spanned as:

$$V_i = V_i^{conf} + V_i^{strain} + V_i^{self}, \tag{3}$$

where V_i^{conf}, V_i^{strain} and V_i^{self} stand for the spatial confining potential, strain deformation potential and self-energy interaction potential, respectively. V_i^{conf} is defined by the band offset between the core and the crown or surrounding materials. It is taken to be zero inside the core, a value defined by the (bulk) band offset in the crown (see Table. 1 below) and 2.5 eV in the outer matrix (representing insulating organic ligands). V_i^{strain} is taken as the diagonal term of the deformation potential in k·p Hamiltonians, see Ref. 1 for details. V_i^{self} is described within the image charge method for infinite quantum wells,[2] as lateral dielectric confinement is comparatively much weaker in NPLs owing to the large shape anisotropy.

Coulomb interaction terms, $V_c(\mathbf{r}_i)$, are calculated by integrating the Poisson equation within an inhomogeneous dielectric environment, using Comsol Multiphysics 4.2. Many-body eigenstates and eigenenergies are then calculated within a full CI method,[3] exploiting

permutation and spin S_z symmetries, using *CItool* codes.[4] The CI basis set is formed by all possible combinations of the first 20 independent-electron and 24 independent-hole spin-orbitals

Regarding material parameters, low temperature band gaps of CdSe (1.76 eV) and CdTe (1.6 eV) and band offsets potentials (Table 1) are taken from Ref. 5. The NPL relative dielectric constant is set to $\varepsilon_{in} = 10$ and that of the outer medium (if dielectric mismatch is considered) to $\varepsilon_{out} = 2$. These are reasonable values for Cd chalcogenide NPLs and typical ligands, which reproduce well experimentally observed trion binding energies, to name an example.[6] The rest of parameters are given in the supporting information of Ref. 1. We note that the value of the conduction band offset for CdSe/CdS is sometimes considered to be uncertain, with some studies suggesting it could be negligible.[7] If we used a lower band offset than 0.24 eV in our simulations, the situation would be essentially equivalent to that of a CdSe/CdS NPL with a somewhat larger core, so the same conclusions would hold.

Table 1: CdSe/CdS and CdSe/CdTe band offset values.

Band Offsets (eV)	
Conduction Band Offset (CBO)	
CdSe/CdS	CdSe/CdTe
0.24	0.53
Valence Band Offset (VBO)	
CdSe/CdS	CdSe/CdTe
0.48	-0.69

Thermal occupation is simulated by the Fermi-Dirac thermal population distribution on the stationary states. The spin for equal population of high and low spins is obtained as $\langle S_e \rangle_{eq} = \frac{M^l S^l + M^h S^h}{M^l + M^h}$ where S^l (S^h) is the spin of the low (high) spin states that can be formed with N electrons (e.g. $S = 0$ and $S = 1$ for $N = 2$), and $M^{i=l,h}$ the corresponding spin multiplicities.

Additional calculations

Addition energies and spin of few fermion systems

In Fig. S1 we plot the difference between the addition energies of interacting and non-interacting carriers, as inferred from Fig.2 of the main text. In a perturbative scheme, where electron-electron (or hole-hole) Coulomb integrals were approximately constant for different values of N_e (N_h), the repulsive terms in Δ would compensate (see Eq. 1 of the main text) and one would expect a roughly constant value of the figure. It is quite clear from the figure, however, that this is not the case.

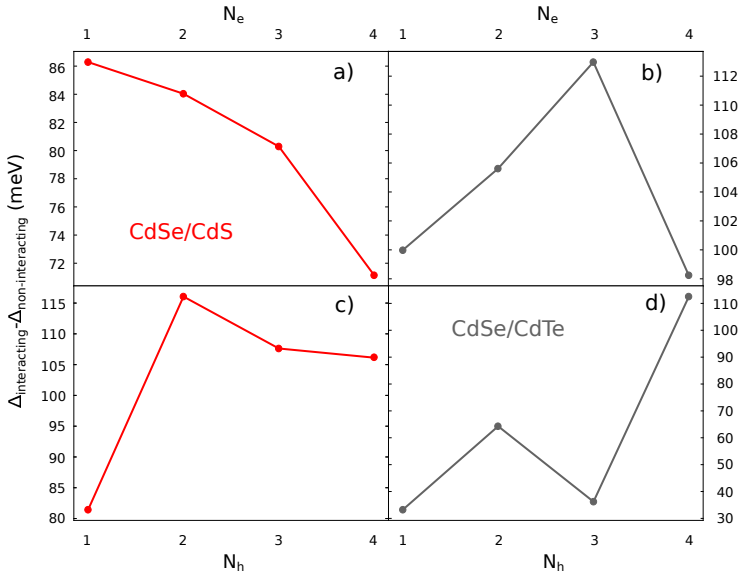

Figure S1: Difference between addition energy spectra of interacting and non-interacting particles in NPLs with $L_y^c = 20$ nm. (a) Electrons in CdSe/CdS NPLs. (b) Electrons in CdSe/CdTe NPLs. (c) Holes in CdSe/CdS NPLs. (d) Holes in CdSe/CdTe NPLs. The interacting case is that including dielectric mismatch (Fig.2c and 2f in the main text).

For electrons in CdSe/CdS nanoplatelets (panel a), the difference decreases monotonically as N_e increases. This suggests electrons are leaking outside the core to reduce repulsions (even if the single-particle orbitals in Fig.1b of the main text would suggest more electrons can fit inside the core). For electrons in CdSe/CdTe (panel b) and for holes in both materials (panels c and d), the changes are non-monotonic, because the confinement potential (band

offset) is more rigid, and the interplay between correlation and lateral confinement becomes more complicated.

In general, the figure evidences changes of 15 meV for electrons, and much more for holes (over 100 meV for the CdSe/CdTe core-crown platelets). This variation is a hint of the strong electronic correlations taking place in the system (about 15% of the total addition energy). In the case of holes in CdSe/CdTe, the differences also reflect the non-simple (diatomic-like) confinement potential.

The addition energies presented in Fig. 2 of the manuscript correspond to NPLs with a $L_y^c = 20$ nm core. Fig. S2 shows that electron and hole addition energies greater than room temperature thermal energy are also obtained for smaller core sizes (notice that in our model smaller cores imply larger crowns).

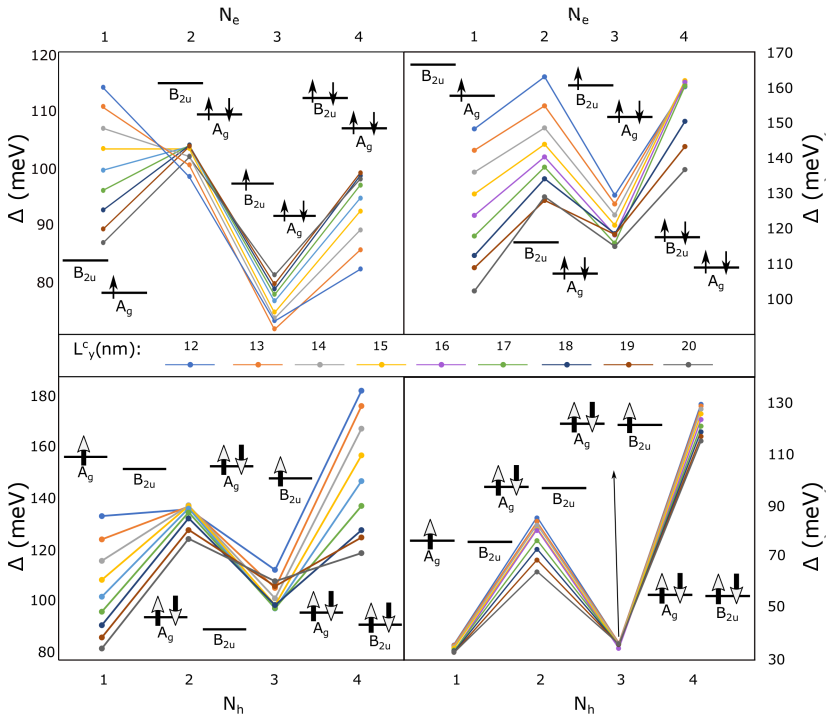

Figure S2: Addition energy spectra as a function of the number of carriers for interacting electrons (top row) and interacting holes (bottom row) in CdSe/CdS NPLs (left column) and CdSe/CdTe NPLs (right column) with different core lengths, L_y^c.

A shell structure, with maxima at even number of electrons (closed shells) is preserved

in most instances. A relevant exception takes place for electrons in CdSe/CdS NPLs with $L_y^c < 15$ nm. In such a case, $N_e = 2$ does not reflect a local maximum in Δ. That is, the closed shell configuration ($N_e = 2$) is less stable than the open shell one ($N_e = 1$). The reason is that, for small enough cores, the lowest single electron orbital is localized in CdSe, but Coulomb repulsions are strong enough as to overcome the band offset and push the second electron into excited orbitals, which are delocalized all over the CdSe/CdS heterostructure. This is a Coulomb-blockade effect.

Fig. S3 shows that thermal occupation of high spin states can be obtained not only in few-electron CdSe/CdS NPLs (Fig. 3 of the main text) but also in CdSe/CdTe NPLs.

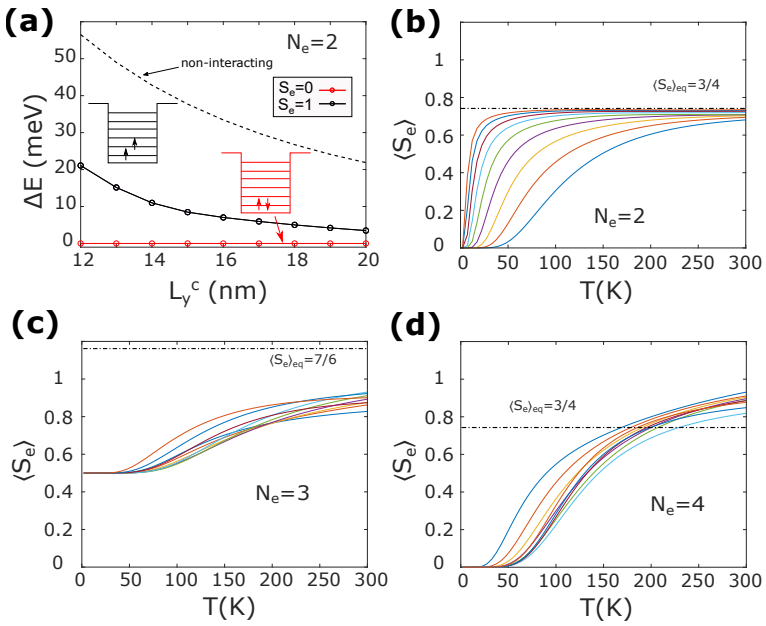

Figure S3: Same as Fig. 3 of the main text, but for CdSe/CdTe NPLs.

Fig. S4 represents the $N_e = 3$ and $N_e = 4$ energy levels for CdSe/CdS and CdSe/CdTe NPLs, as a function of the core size. The ground state corresponds to the lowest possible spin in all cases, but high spin states are generally available at temperatures under ~ 24 meV (room temperature thermal energy). For $N_e = 4$, spin triplet states (black lines) within such an energy range outnumber spin singlet ones (red lines). The higher density of states in CdSe/CdS, as compared to CdSe/CdTe, is due to the low conduction band offset.

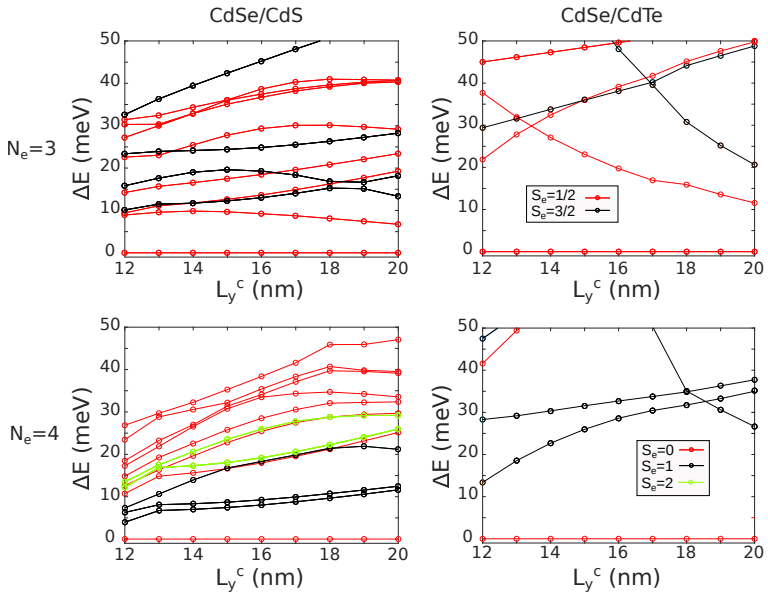

Figure S4: Energy levels as a function of the core length for three and four interacting electrons in CdSe/CdS (left) and CdSe/CdTe (right). Different lines denote different total electron spin. All energies are referred to the ground state for a given core length, L_y^c.

One can note in Fig. S4 that, contrary to the case of $N_e = 2$ electrons (Fig.3 in the main text), high spin states for $N_e = 3$ and $N_e = 4$ do not get closer to the ground state with increasing core length, L_y^c. The reasons is that for $N_e = 2$, the ground state is a singlet with two paired electrons. The triplet state state requires occupying an excited orbital, and the larger the length of the core, the closer this orbital is – see Fig. 3(a) –. For $N_e = 3$ and $N_e = 4$, however, the excited orbital is already occupied in the ground state, so the influence of confinement is less straightforward. This difference explains the opposite trends of $\langle S_e \rangle$ in Fig.3 of the main text: it increases with L_y^c when $N_e = 2$, but it does not when $N_e = 3$ or $N_e = 4$.

References

(1) Llusar, J.; Planelles, J.; Climente, J. I. Strain in Lattice-Mismatched CdSe-Based Core/Shell Nanoplatelets. *The Journal of Physical Chemistry C* **2019**, *123*, 21299–21306.

(2) Kumagai, M.; Takagahara, T. Excitonic and Nonlinear-Optical Properties of Dielectric Quantum-Well Structures. *Phys. Rev. B.* **1989**, *40*, 12359–12381.

(3) Llusar, J.; Climente, J. I. Nature and Control of Shakeup Processes in Colloidal Nanoplatelets. *ACS Photonics* **2020**, *7*, 3086–3095.

(4) Bertoni, A. CItool. `https://github.com/andreabertoni/citool`, 2011; [Online; accessed 4-May-2021].

(5) Adachi, S. *Handbook on Physical Properties of Semiconductors, vol.3*; Kluwer Academics, 2004.

(6) Macias-Pinilla, D. F.; Planelles, J.; Mora-Seró, I.; Climente, J. I. Comparison between trion and exciton electronic properties in CdSe and PbS nanoplatelets. *The Journal of Physical Chemistry C* **2021**, *125*, 15614–15622.

(7) Eshet, H.; Grünwald, M.; Rabani, E. The electronic structure of CdSe/CdS core/shell seeded nanorods: type-I or quasi-type-II? *Nano letters* **2013**, *13*, 5880–5885.